Simulation Studies on Backgrounds in nEXO from Radon-daughter Plate-out

Venkatesh Veeraraghavan,[1, 2, a)] Raymond Hei-man Tsang,[1] and Andreas Piepke[1]

[1)]*Department of Physics and Astronomy, University of Alabama, Tuscaloosa, Alabama 35487, USA*
[2)]*Department of Physics and Astronomy, Iowa State University, Ames, Iowa 50011, USA*

[a)]*Corresponding author: vveeraraghavan@ua.edu*

Abstract. nEXO is a proposed search for neutrinoless double beta decay ($0\nu\beta\beta$) of ^{136}Xe. The experiment is planning to utilize isotopically enriched xenon both as source and detection medium. Radon daughters produced by radon decays in the air can plate out on material surfaces during detector assembly and handling. The alpha particles they emit can interact with low-Z materials nearby and produce fast neutrons. These neutrons can in turn produce ^{137}Xe when captured by ^{136}Xe contained in the nEXO detector medium. The subsequent beta decay of ^{137}Xe ($Q = 4173$ keV) can mimic $0\nu\beta\beta$ in nEXO. This paper describes simulation studies performed to estimate the background in nEXO produced by radon daughters. We will also discuss the allowed amounts of radon daughters on material surfaces in order to meet nEXO's stringent background requirements.

INTRODUCTION

The next-generation Enriched Xenon Observatory (nEXO) is a planned experiment to search for neutrinoless double beta ($0\nu\beta\beta$) decay of ^{136}Xe. The nEXO experiment will conduct the search using a time projection chamber (TPC) and five tonnes of liquid xenon (LXe) that is enriched to 90% in ^{136}Xe. The Q value for ^{136}Xe double-β decay, $Q_{\beta\beta}$, is 2458 keV [1, 2].

The different categories of background in nEXO are intrinsic radioactivity, steady-state ^{222}Rn in LXe, and exposure-based backgrounds, as shown in Fig. 1 [3]. In the exposure-based category, ^{137}Xe background can be created by neutron captures on ^{136}Xe. Three sources of neutrons were considered and studied. High-energy neutrons can be created by cosmic-ray muons that penetrate to the deep underground location that hosts the nEXO experiment. Low-energy neutrons created by energetic α-particles interacting with nuclei in nearby low-Z materials are also a concern. Radon daughter plate-out is a source of energetic α-particles in turn creating low-energy neutrons. Energetic α-particles present in the uranium and thorium decay chains can also create low-energy neutrons in nEXO detector materials. We evaluated background rates from αs present in the uranium and thorium decay chains and found them to be negligible relative to the rate from γs in the same decay chains. The focus of this paper is the simulation study of backgrounds induced by radon-daughter plate-out. We discuss the background mechanism and simulation studies, and we provide limits on initial conditions that would render this source of background to be a small fraction of the total background budget of the nEXO experiment. If these initial conditions are achieved, then the only relevant contributor to the ^{137}Xe background in nEXO will be that from cosmic muons, as shown in Fig. 1.

The current estimate for the number of single-site background events in the inner two tonnes of nEXO, in the energy interval $Q_{\beta\beta} \pm \mathrm{FWHM}/2$, for one year of data taking is 0.5. The full width at half maximum (FWHM) energy window around $Q_{\beta\beta}$ for the study presented in this paper is 2428 – 2488 keV. Given the small expected background count, it is imperative to evaluate all plausible backgrounds and their associated dependencies. Neutrons, for instance from radon-daughter plate-out, have a larger mean free path in LXe than γ-rays and can disrupt the highly clean central region of the TPC. Attachment rates for radon-daughter plate-out have dependencies that are not well understood, necessitating a careful assessment of this class of background. The attachment rates are being studied too but are not covered in this article.

RADON-DAUGHTER PLATE-OUT MECHANISM

Charged ^{222}Rn daughters can attach to surfaces of materials that are used for the nEXO experiment when they are exposed to radon-containing air. ^{222}Rn daughters have been found to be soluble in cryogenic fluids such as HFE-7000 (manufactured by 3M with chemical formula $C_3F_7OCH_3$). Within the ^{222}Rn decay chain (Fig. 1), all nuclides until ^{210}Pb have short half-lives relative to the time needed to assemble the nEXO detector and to begin operations. Therefore, ^{222}Rn daughters that attach to surfaces of nEXO materials decay and result in continual constant accumulation

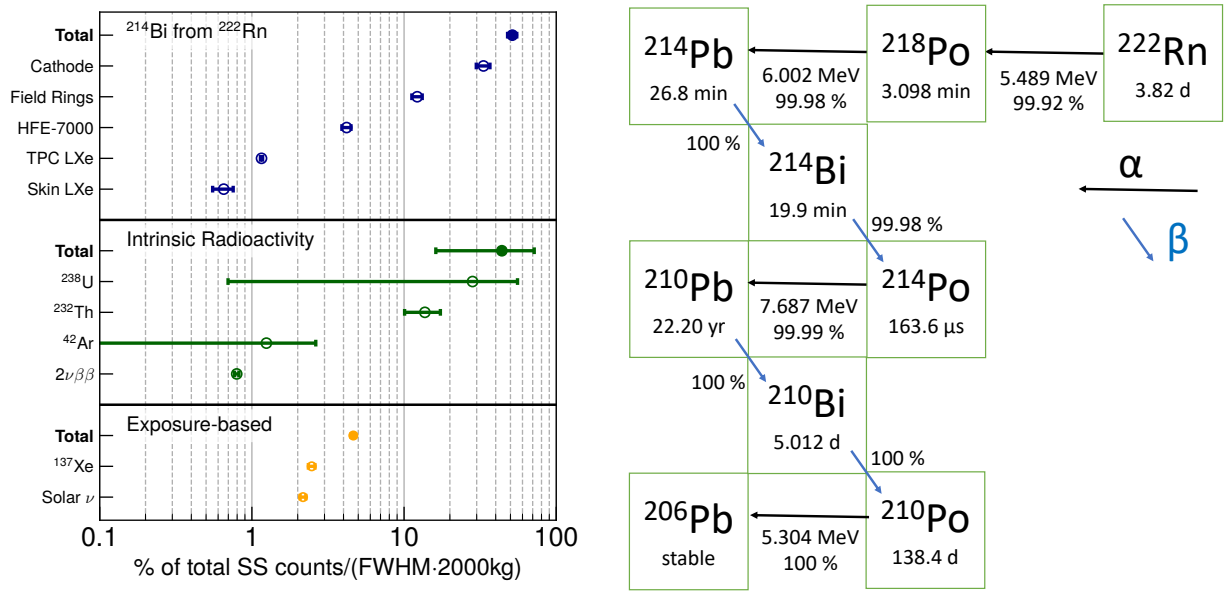

FIGURE 1. **Left:** Single-site-like fractional background contributions with energy within $Q_{\beta\beta} \pm$ FWHM/2 and in the inner 2000 kg of nEXO detector [3]. The background due to ^{137}Xe assumes sources of it described in this paper are kept small compared to that from cosmic muons. **Right:** ^{222}Rn decay chain.

of ^{210}Pb on exposed surfaces. The decay of ^{210}Pb, in turn, results in the growth of ^{210}Po which then decays with the emission of a 5.3-MeV α-particle. The said α-particle can then interact with low-Z nuclei that are present in its vicinity and expel neutrons from them. A specific example of the aforementioned scenario is ^{222}Rn daughters attaching to TPC vessel copper surfaces and then the α-particle resulting from ^{210}Po decay interacting with carbon, oxygen, and fluorine nuclei that are present in nearby HFE-7000. The neutrons resulting from the (α, n) nuclear reactions can then traverse the nEXO detector and create background events in the active LXe either directly or via neutron capture. In particular, neutron capture on ^{136}Xe results in ^{137}Xe which then undergoes β-decay with a Q value of 4173 keV. These interactions can yield single-site events in the energy window relevant to the nEXO experiment.

Background estimates due to radon-daughter plate-out are directly dependent on the exposure time of nEXO materials to surface conditions. We can determine the limit on exposure time that will render each radon-daughter plate-out background to be below some threshold. A literature survey of radon-daughter attachment-rate studies yields a wide range of results. Dependencies on environmental conditions are often not well understood. We decouple the uncertain part and present results in terms of limits on the allowed ^{210}Po specific activity, $A^{\text{all.}}_{^{210}\text{Po}}$, in or on nEXO materials.

We describe background rate calculation from initial conditions in the next section. Studies done to determine various terms in the rate calculation are discussed in subsequent sections. Since initial conditions are unknown, we invert the rate calculation to determine limits on initial conditions that would render this class of background to be a small fraction of the current nEXO background budget.

We studied seven cases of radon-daughter plate-out background. They cover cases where radon daughters are either attached to the surface of some nEXO detector part or dissolved in the bulk of some nEXO detector component. For surface activity, the α-particle from ^{210}Po decay interacts with low-Z nuclei in a nearby material, for a bulk activity with the host material itself.

BACKGROUND RATE CALCULATION

The background rate for a given component due to ^{210}Po,

$$B_{210\text{Po}} = A_{210\text{Po}} \times \sigma \times \varepsilon_{\text{distrib.}} \times Y_{\text{n}} \times \varepsilon_{\text{n}}, \tag{1}$$

TABLE I. Target-nuclide specific ratios of neutron production yield and average neutron energy, evaluated for equal stopping media but different cross-section sets with SOURCES-4C.

Nuclide	Y_n^{upd}/Y_n^{orig}	$\langle E_n^{upd}\rangle/\langle E_n^{orig}\rangle$
^{13}C	1.05	1.01
^{17}O	0.98	1.002
^{18}O	1.01	1.001
^{19}F	0.97	0.99
^{27}Al	1.23	1.007
^{29}Si	0.63	0.935
^{30}Si	0.58	1.32

where A_{210Po} is the ^{210}Po specific activity, σ is the component's surface area or mass, $\varepsilon_{\text{distrib.}}$ is the phase-space factor (0.5 for ^{222}Rn daughter attachment to surfaces and 1.0 for ^{222}Rn daughters dissolved in volumes or fluids), Y_n is the number of neutrons that are expelled per α-particle (also referred to as neutron yield), and ε_n is the efficiency of neutrons to create a single-site event in the FWHM energy window in the inner two tonnes of nEXO. For each background case, we calculated the neutron yield and did simulation studies of the neutrons in the nEXO detector. We expand on both these aforementioned studies in the next two sections. We then invert Eq. 1 to determine the limits on A_{210Po} that would render the studied background to be a small fraction of the total nEXO background budget.

Neutron yield

Interactions of α-particles with low-Z nuclei in nEXO-detector parts were studied using the SOURCES code package [4]. nEXO construction materials with nuclear charge $Z > 14$ were determined not to be a concern for radon-daughter plate-out backgrounds. For atoms with $Z > 14$, the electric repulsion between the approaching α-particle and target atomic nucleus results in reaction thresholds that exceed the kinetic energy of the α-particles emitted in ^{210}Po decays. The SOURCES code is provided by the Los Alamos and Oak Ridge National Laboratories. Version 4C was used for this work. Several modifications were made to SOURCES-4C for the work presented here. The (α, n)-cross sections for ^{13}C, ^{16}O, ^{17}O, ^{18}O, ^{19}F, ^{27}Al, ^{29}Si, and ^{30}Si were replaced by more modern data, derived from the JENDL-2005/AN and TENDL 2009 databases. The energy range was extended from 6.5 MeV to 15 MeV. This energy range enhancement enables studies other than the one presented here, such as modeling of α-particles in the entire ^{238}U and ^{232}Th chains.

Because the code was modified with updated (α, n)-cross sections, its functionality was verified using a numerical stand-alone calculation. For the numerical calculation, we used α energy-dependent mass stopping powers provided by NISTS's ASTAR online database. Table I shows ratios of (α, n)-production yields and average neutron energies, $\langle E_n\rangle$, evaluated with SOURCES-4C for equal stopping media with the original and updated cross sections. Most nuclides show only little change, but there are exceptions.

For all studied background cases, we list details of ^{222}Rn-daughter attachment to surfaces or volumes and the corresponding low-Z target material in Tab. II. The energy distribution for neutrons created in HFE-7000 is shown in Fig. 2. Locations of neutron creation and the neutron energy distribution are used as input to the GEANT4 simulation of the nEXO detector response that are discussed in the next section.

Neutron Efficiencies

Detector simulations were done with neutrons situated in appropriate locations in the nEXO detector (Tab. II) and their energies randomly sampled over the distributions derived in the previous section. The physics list "Shielding" was used in simulations to enable all low-energy hadronic interactions with high precision. As neutrons traverse the nEXO detector, they undergo elastic and inelastic scattering and can be captured. Neutron capture can happen anywhere in nEXO detector, but we only studied neutron captures in xenon. Among the disintegrations that follow neutron capture in LXe, only ^{137}Xe disintegrations yield energies overlapping the $Q_{\beta\beta} \pm \text{FWHM}/2$ energy window. The simulations are split into two parts. In the first part, we determine the efficiency of neutrons to produce direct backgrounds and

TABLE II. List of radon-daughter plate-out backgrounds that were studied. For each studied background, neutron yield Y_n along with location of neutrons in subsequent GEANT based simulations are also listed.

^{222}Rn-daughter attachment		Low-Z target material		Y_n	Neutron location
Material	nEXO component	Low-Z target nuclides	nEXO component	(10^{-8})	
Copper	TPC vessel	^{13}C, ^{17}O, ^{18}O, ^{19}F	HFE-7000	511	HFE-7000 skin enveloping TPC vessel
HFE-7000	HFE-7000	^{13}C, ^{17}O, ^{18}O, ^{19}F	HFE-7000	511	HFE-7000
Titanium	Inner cryostat liner	^{13}C, ^{17}O, ^{18}O, ^{19}F	HFE-7000	511	HFE-7000 skin near inner cryostat liner
Sapphire	Field cage spacers	^{17}O, ^{18}O, ^{27}Al	Field cage spacers	33.2	Field cage spacers
Silicon	SiPMs	^{29}Si, ^{30}Si	SiPMs	7.3	SiPMs
Quartz	Charge tile backing	^{17}O, ^{18}O, ^{29}Si, ^{30}Si	Charge tile backing	6.7	Charge tile backing
Quartz	Interposer	^{17}O, ^{18}O, ^{29}Si, ^{30}Si	Interposer	6.7	Interposer

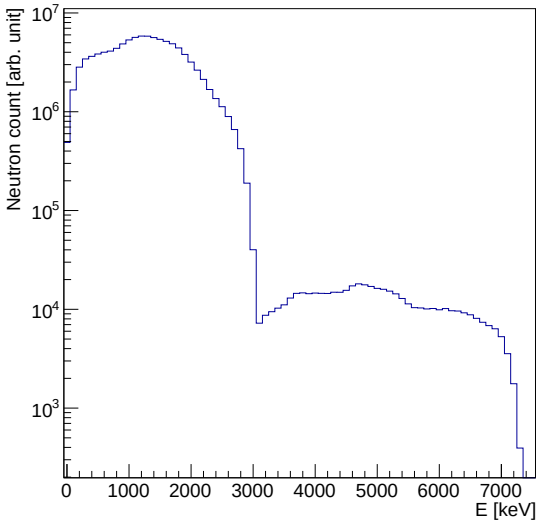

FIGURE 2. Distribution of energies of neutrons produced in HFE-7000 by interactions of alphas from radon daughters.

the efficiency of neutrons to capture on ^{136}Xe to create ^{137}Xe. In the second part, we determine the efficiency of the ^{137}Xe decays to produce backgrounds.

Neutron simulations were done with the following setting

/grdm/nucleusLimits 136 136 54 54

so that decays other than that of $^{136}_{54}$Xe are forbidden. The half-life of ^{137}Xe is 3.8 minutes and if ^{137}Xe disintegrations were to be simulated in continuation of neutron action within the same event, then it would result in the addition of energies from separate events. Also, ^{137}Xe β-decay events that will mostly be single-site events would be recorded as multi-site events. Both these features would result in an underestimation of the background. Therefore, ^{137}Xe disintegrations that are caused by neutron action in nEXO detector are simulated separately.

During neutron simulations, energy deposits in LXe and $(x,\ y,\ z)$ coordinates of neutron captures on ^{136}Xe were recorded. Energy deposits during neutron interactions in LXe were clustered and reconstructed utilizing standard nEXO algorithms. Capture sites in LXe have azimuthal-symmetry. However, there are more captures close to the TPC boundary than in the inner regions, along both radial and longitudinal directions. Neutron captures in LXe can also be presented in terms of standoff distances, defined as the distance to the nearest xenon surface, and this approach eases the integration of the subsequent step of ^{137}Xe simulations.

The LXe contained in the nEXO TPC will be continually recirculated and purified. The process of xenon recirculation will, on average, reduce the observed inhomogeneity of neutron captures in ^{136}Xe. However, the current estimate

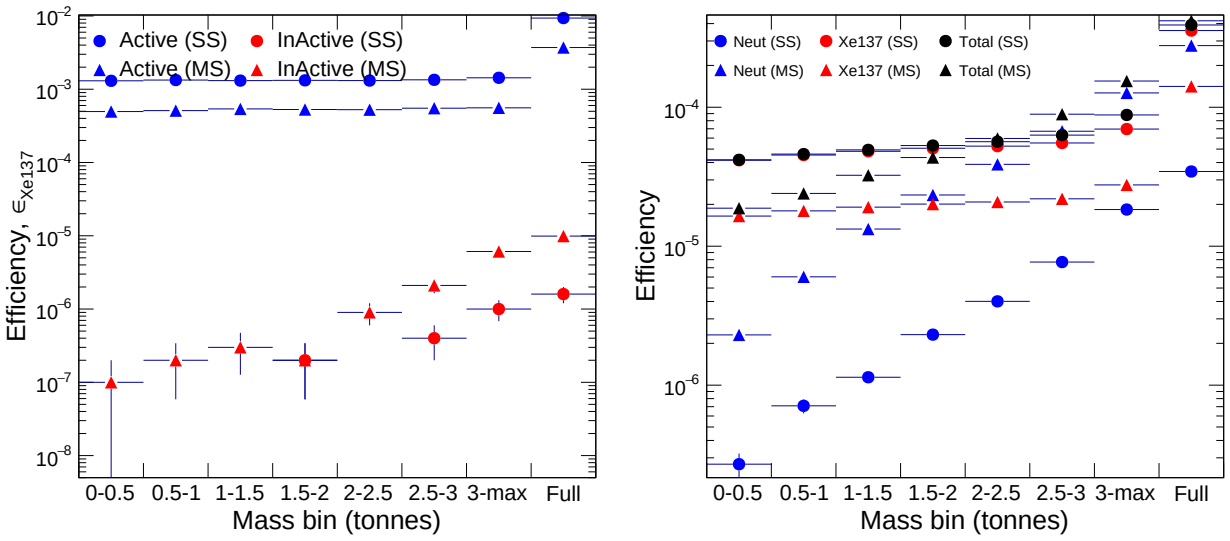

FIGURE 3. Left: Fraction of uniformly-distributed ^{137}Xe disintegrations occurring in the active (blue) or inactive (red) LXe that yields events in the FWHM energy window in various detector regions, $\epsilon_{\mathrm{Xe137}}$. The first bin is the central 0.5 tonnes of xenon, the second bin is the xenon in the next 0.5 tonnes out from the center, and so on. The rightmost bin gives the efficiency summed over the full detector. **Right:** Efficiency for neutrons generated in the HFE-7000 skin enveloping the TPC vessel to create single-site and multi-site events in the FWHM energy window in various detector regions. Efficiencies are shown for neutron action, for neutron-capture-induced ^{137}Xe disintegration, and for their sums.

for one complete xenon recirculation period is four days. Given that the half-life of ^{137}Xe is 1500 times shorter than the LXe purification period, the effect of circulation on neutron capture non-homogeneity is considered negligible.

To determine the effect of ^{137}Xe disintegrations, we simulated uniform ^{137}Xe disintegrations in both active LXe and inactive LXe. The hit efficiency for ^{137}Xe disintegrations that are uniformly distributed in both active LXe and inactive LXe in the FWHM window in equally-sized detector regions is presented in Fig. 3. Based on the fact that efficiencies do not vary when comparing differently-situated but equally-sized detector regions, we infer that the efficiency for a ^{137}Xe disintegration to yield an event in the same location as the parent decay and within the FWHM energy window is uniform across the entire detector region. This is not unexpected as ^{137}Xe β-decays are localized. Using this feature, the number of neutron captures on ^{136}Xe in the inner two tonnes can be used to obtain the number of events in the FWHM energy window by multiplication with an efficiency number, $\epsilon^{\mathrm{SS}}_{\mathrm{Xe137}} = 9.36 \times 10^{-3}$, instead of a function.

As seen from Fig. 3, ^{137}Xe disintegrations in the inactive LXe, relative to active LXe, contribute 1000 times less events to the FWHM energy window. For all studied radon-daughter plate-out cases, the much smaller efficiency of the inactive LXe is not compensated by the number of neutron captures. Therefore we do not explore captures in inactive LXe any further.

The efficiency of neutrons to yield single-site background events within $Q_{\beta\beta} \pm \mathrm{FWHM}/2$ and in the inner two tonnes of xenon can be expressed as

$$\epsilon_{\mathrm{n}} = \epsilon^{\mathrm{SS}}_{\mathrm{n}} + \epsilon^{\mathrm{Xe136}}_{\mathrm{n}} \times \epsilon^{\mathrm{SS}}_{\mathrm{Xe137}}, \tag{2}$$

where the first term, $\epsilon^{\mathrm{SS}}_{\mathrm{n}}$, is the efficiency for neutrons to directly create a background event (e.g. via elastic or inelastic scattering), the second term is the product of the probability for neutrons to be captured by ^{136}Xe ($\epsilon^{\mathrm{Xe136}}_{\mathrm{n}}$) and the efficiency of the subsequent ^{137}Xe disintegration to create a background event ($\epsilon^{\mathrm{SS}}_{\mathrm{Xe137}}$). For the purpose of background determination, the efficiencies are evaluated for single-site events in the inner two tonnes. For neutrons generated in the HFE-7000 skin enveloping the TPC vessel, Fig. 3 shows ϵ_{n} in various detector volumes. Note in Fig. 3 that the neutron background is dominated by capture on ^{136}Xe. We list ϵ_{n} for all background cases in the next section.

RESULTS

We use neutron yields and efficiencies in the background-rate equation (Eq. 1) to derive numerical values for "allowable" amounts of ^{210}Po on surfaces or in the bulk of materials to be used in nEXO. Each background category in nEXO is assigned a fraction of the total background budget. Table III lists Y_n, ε_n, and $A^{\text{all.}}_{^{210}\text{Po}}$, defined so that the sum of all these background components is 0.5% of the expected detector background rate of 0.5 events per year in nEXO's inner two tonnes.

TABLE III. Various efficiencies and "allowable" values of ^{210}Po specific activity for all studied background cases. Numbers in parenthesis are uncertainties expressed as a percentage.

nEXO component	Y_n (10^{-8})	ε_n (10^{-4})	Area or Mass	$A^{\text{all.}}_{^{210}\text{Po}}$	
				Value	Units
TPC vessel	511	1.9 (0.7%)	7.84 m^2	4.7	mBq/m^2
HFE-7000 bulk	511	0.2 (2.3%)	31814 kg	58	μBq/kg
Inner cryostat liner	511	7.3×10^{-4}(37%)	40.72 m^2	2.4	Bq/m^2
Field cage spacers	33.2	2.2 (0.7%)	0.50 m^2	1.0	Bq/m^2
SiPMs	7.3	2.2 (0.7%)	11.43 m^2	0.2	Bq/m^2
Charge tile backing	6.7	1.9 (0.7%)	2.54 m^2	1.1	Bq/m^2
Interposer	6.7	2.1 (0.7%)	11.43 m^2	0.22	Bq/m^2

SUMMARY

We studied seven cases of neutron background caused by radon-daughter plate-out. For each case, initial-state conditions that would render the background to be "allowable" as defined above were derived. Ultimately, the aforementioned initial-state conditions define maximum time-periods of exposure of nEXO detector materials to different radon environments. To decouple the uncertain ^{222}Rn-daughter attachment properties from the solid rate calculations, we derived "allowable" values of the ^{210}Po specific activities instead. While it is not expected to be a major background source, nEXO is devising ways to measure ^{210}Po contamination on surfaces and in bulk volumes.

ACKNOWLEDGMENTS

This work was conceived as a contribution to the development of the nEXO experiment. The authors acknowledge the use of nEXO collaboration computing resources and software for the detector modelling discussed in this paper. We thank our nEXO colleagues for their support. This research was supported in part by the U.S. Department of Energy under DOE Grant DE-FG02-01ER41166.

REFERENCES

1. M. Redshaw, E. Wingfield, J. McDaniel, and E. G. Myers, "Mass and double-beta-decay Q value of ^{136}Xe," Phys. Rev. Lett. **98**, 053003 (2007).
2. P. M. McCowan and R. C. Barber, "Q value for the double-β decay of ^{136}Xe," Phys. Rev. C **82**, 024603 (2010).
3. G. Adhikari *et al.* (nEXO Collaboration), "nEXO: neutrinoless double beta decay search beyond 10^{28} year half-life sensitivity," J. Phys. G: Nucl. Part. Phys. **49**, 015104 (2021), arXiv:2106.16243v2 [nucl-ex].
4. W. B. Wilson, R. T. Perry, E. F. Shores, W. S. Charlton, T. A. Parish, G. P. Estes, T. H. Brown, E. D. Arthur, M. Bozoian, T. R. England, D. G. Madland, and J. E. Stewart, "Sources 4c : a code for calculating ([alpha],n), spontaneous fission, and delayed neutron sources and spectra." (2002), `https://www.osti.gov/biblio/976142`.